Journal of The Electrochemical Society, **161** (6) C363-C371 (2014)
0013-4651/2014/161(6)/C363/9/$31.00 © The Electrochemical Society

The Anodic Reactions on Simulated Spent Fuel (SIMFUEL) in H_2O_2 Solutions: Effect of Carbonate/Bicarbonate

Linda Wu,* Jon S. Goldik, and David W. Shoesmith,z**

Department of Chemistry and Surface Science Western, The University of Western Ontario, London, Ontario N6A 5B7, Canada

The anodic behavior of simulated nuclear fuel (SIMFUEL) in solutions containing H_2O_2 and HCO_3^-/CO_3^{2-} has been studied electrochemically and using surface analytical techniques, in particular X-ray photoelectron spectroscopy. Two anodic reactions are possible, the oxidative dissolution of UO_2 and H_2O_2 oxidation. The rates of both reactions are controlled by the chemical release of U^{VI} surface species, and can both be increased by the addition of HCO_3^-/CO_3^{2-}. Under anodic conditions the dominant reaction is H_2O_2 oxidation, although UO_2 dissolution may also be accelerated by the formation of a uranyl peroxocarbonate complex. Similarly, under open circuit (corrosion) conditions both UO_2 corrosion and H_2O_2 decomposition are also controlled by the rate of release of U^{VI} surface species which blocks access of H_2O_2 to the underlying conductive $U^{IV}_{1-2x}U^{V}_{2x}O_{2+x}$ surface. Presently, the balance between these two reactions is not known.

Manuscript submitted March 31, 2014; revised manuscript received May 7, 2014. Published May 19, 2014. This was Paper 1605 presented at the Boston, Massachusetts, Meeting of the Society, October 9–14, 2011.

The recommended approach for the long-term management of spent nuclear fuel in Canada is adaptive phased management that includes centralized containment and the isolation of the spent fuel in a deep geological repository. The repository concept is based on multiple barriers including the fuel bundles, durable metal containers with an outer barrier of copper and an inner carbon steel liner, a clay buffer and seals around the container, and a deep geologic environment.[1] A key barrier is the corrosion-resistant container that is designed to isolate the spent fuel from groundwater until radiation levels in the fuel become insignificant.[2,3] However, it is judicious to examine the consequences of early container failure leading to the exposure of spent fuel bundles to groundwater. In the anoxic conditions anticipated in a deep geological repository, water radiolysis resulting from the radiation fields associated with fuel will be the only source of oxidants required to drive fuel oxidation. Oxidation of fuel (U^{IV}) will produce U^{VI} which is considerably more soluble than U^{IV}, and its subsequent dissolution will lead to the release of radionuclides.[4] The alpha radiolysis product, H_2O_2, is expected to be the primary driving force for fuel corrosion.[5–7]

The fuel corrosion rate will also be influenced by the groundwater composition. For a Canadian deep geologic repository,[8] the major groundwater species will be $Ca^{2+}/Na^+/Cl^-/SO_4^{2-}$ with a small amount of HCO_3^-/CO_3^{2-} (10^{-4} to 10^{-3} mol L^{-1}). The groundwater pH will be in the range 6 to 10. The key groundwater species likely to accelerate fuel corrosion is HCO_3^-/CO_3^{2-} which is a strong complexing agent for the $U^{VI}O_2^{2+}$ ion.[4,9,10] The influence of HCO_3^-/CO_3^{2-} has been investigated in both chemical[11–14] and electrochemical dissolution experiments.[15–17] A carbonate concentration $\geq 10^{-3}$ mol L^{-1} was found to prevent the deposition of U^{VI} corrosion products on the UO_2 surface leading to a significant increase in the corrosion rate. When a sufficient HCO_3^-/CO_3^{2-} concentration was present the formation of the underlying $U^{IV}_{1-2x}U^{V}_{2x}O_{2+x}$ film, which forms prior to the onset of dissolution,[5,18] is also inhibited.[11,12]

Two anodic reactions are possible on an active UO_2 surface; oxidative dissolution of the UO_2 and H_2O_2 oxidation. The latter reaction can couple with H_2O_2 reduction resulting in its decomposition to H_2O and O_2. Consequently, the corrosion rate of fuel will be determined by the distribution of current between these two anodic reactions. Although the cathodic reduction of H_2O_2 on UO_2 has been extensively investigated,[19–23] its anodic oxidation has received minimal attention.

Attempts have been made to determine the mechanistic balance between UO_2 dissolution and H_2O_2 decomposition under open circuit (corrosion) conditions.[5,15] At low $[H_2O_2]$ ($< 10^{-4}$ mol L^{-1}) the open circuit (or corrosion) potential, E_{CORR}, increased from ~–0.4 V to ~0.1 V (vs. SCE) with increasing $[H_2O_2]$, and recent studies showed that the value of the steady-state E_{CORR} achieved was directly related to the extent of oxidation of the surface (determined by X-ray photoelectron spectroscopy).[24] Over the intermediate $[H_2O_2]$ range, 10^{-4} to 5×10^{-3} mol L^{-1}, E_{CORR} became independent of $[H_2O_2]$, a situation suggesting the dominant surface reaction could be H_2O_2 decomposition rather than H_2O_2-driven UO_2 corrosion. In this concentration range E_{CORR} rose rapidly to the final steady-state value (~0.1 V) indicating that the oxidation step, $U^{IV}O_2$ to $U^{IV}_{1-2x}U^{V}_{2x}O_{2+x}$, was rapid. At potentials in this range both oxidative dissolution as $U^{VI}O_2^{2+}$ and H_2O_2 decomposition are possible. Based on the independence of E_{CORR} on $[H_2O_2]$, it was claimed that the corrosion of the surface and the decomposition of H_2O_2 on the $U^{IV}_{1-2x}U^{V}_{2x}O_{2+x}$ layer were both limited by the slow dissolution of U^{VI} species from a U^{VI} surface layer. XPS measurements confirmed the presence of U^{VI} on the electrode surface in this potential range.

For $[H_2O_2] \geq 5 \times 10^{-3}$ mol L^{-1}, E_{CORR} increased approximately linearly with concentration and coverage of the electrode by U^{VI} species increased. Experiments in which the amount of dissolved U^{VI} was measured showed that, at these higher $[H_2O_2]$ dissolution was accelerated[20,25] and the rate became first order with respect to $[H_2O_2]$. This increase in dissolution rate coupled to an apparently greater coverage by insulating and potentially blocking surface U^{VI} species was taken as an indication of enhanced dissolution at locally acidified sites on the electrode surface.[15] How these changes influenced the rate and extent of H_2O_2 decomposition was not investigated. A similar mechanism was proposed for the influence of α-radiolytically produced H_2O_2 on UO_2 corrosion and H_2O_2 decomposition.[26] It has also been claimed that, in the presence of both H_2O_2 and HCO_3^-/CO_3^{2-} at high concentrations, UO_2 corrosion is accelerated due to the formation of a soluble peroxocarbonate complex, $UO_2(O_2)_x(CO_3)_y^{2-2x-2y}$.[27,28]

The decomposition of H_2O_2 on UO_2 has been reported,[15,29,30] measurements of the extents of UO_2 dissolution and H_2O_2 consumption showing that not all the H_2O_2 consumed caused dissolution.[31] When carbonate was present and dissolution unimpeded by deposits,[6,7,32] the discrepancy between UO_2^{2+} release and H_2O_2 consumption indicated that only a fraction of the H_2O_2 consumed lead to UO_2 dissolution, the remainder being decomposed on the UO_2 surface. The fraction of H_2O_2 consumption causing dissolution varied with different UO_2 specimens.[33,34]

The carbonate-mediated decomposition of H_2O_2 has also been reported, the decomposition rate on Ag_2O, Pt, and Pd being shown to increase by a factor of 2 to 3 in K_2CO_3 compared to the rate measured in KOH solutions, while the opposite trend was observed on precipitated silver.[35] Navarro et al.[36] also observed an enhanced

*Electrochemical Society Student Member.
**Electrochemical Society Fellow.
zE-mail: dwshoesm@uwo.ca

decomposition in CO_2/air-purged alkaline solutions which they attributed to the formation of an unstable intermediate, peroxycarbonic acid (H_2CO_4). Csanyi and Galbacs,[37] however, reported that the enhanced rate due to CO_2 disappeared in purified solutions and suggested the catalytic effect observed[36] was due to the presence of trace transition metal carbonato complexes. This was supported by Lee et al.[38] who found the decomposition rate was 9 times faster in Na_2CO_3 than in NaOH solutions when trace levels of metals (<1 ppm wt) were present. Richardson et al.[39] showed that HCO_3^- can activate H_2O_2 in the oxidation of sulfides via the formation of HCO_4^-, since the second order rate constants for sulfide oxidation by HCO_4^- were ~300-fold greater than those for H_2O_2. Suess and Janik[40] and Wu et al.[41] reported that H_2O_2 decomposition was significantly accelerated in aqueous system by adding HCO_3^-/CO_3^{2-} at high temperatures (50–90°C), and attributed this to the formation of active CO_4^{2-}. Despite these endeavors whether or not HCO_3^-/CO_3^{2-} promotes H_2O_2 decomposition under the nuclear waste disposal conditions remains unresolved.

Here we present a study of the influence of H_2O_2 and HCO_3^-/CO_3^{2-} on the competition between H_2O_2 oxidation and UO_2 dissolution using electrochemical and solution/surface analyzes. In addition, the influence of HCO_3^-/CO_3^{2-} on the rate of H_2O_2 decomposition under open circuit conditions has been investigated.

Experimental

A conventional three electrode, three compartment electrochemical cell was used for all experiments. The reference electrode was a saturated calomel electrode (SCE) and all potentials in this paper are quoted on the SCE scale. The counter electrode was a Pt sheet with a surface area of 6 cm^2 spot-welded to a Pt wire. The cell was placed in a grounded Faraday cage to minimize interferences from external noise.

The working electrodes were made from simulated spent fuel pellets (SIMFUEL) fabricated by Atomic Energy of Canada Limited (Chalk River, Ontario). SIMFUELs are stoichiometric UO_2 doped with a series of non-radioactive fission products (Pd, Mo, Ru, Rh, Nd, Ce, Zr, Sr, Ba, La, Y) to simulate in-reactor irradiation.[42] The SIMFUEL used in this study mimics an in-reactor burn-up of 1.5 atomic% which is typical for CANDU fuel. The procedure for electrode preparation has been described previously.[21] The electrodes were polished on wet 1200 grit SiC paper and rinsed with deionized water prior to use. The working electrode was cathodically cleaned at an applied potential of –1.2 V for 2 min prior to an experiment in order to remove any air-formed oxides.

All experiments were conducted in Ar-purged solutions (Praxair) at room temperature. The solutions were prepared using deionized water (18.2 MΩ cm) purified using a Millipore milli-Q-plus unit. The base electrolyte was 0.1 mol L^{-1} NaCl. The total carbonate concentration ($[CO_3]_{tot}$) was adjusted with Na_2CO_3 and $NaHCO_3$ (Caledon Chemical) ranging from 10^{-4} to 2×10^{-1} mol L^{-1}, and the solution pH was adjusted, when required, using 0.1 mol L^{-1} NaOH (Caledon Chemical). Hydrogen peroxide (3% w/v, LabChem Inc.) was added immediately prior to an experiment to a specific concentration in the range from 2×10^{-4} to 2×10^{-2} mol L^{-1}. An Orion model 250A+ pH meter and Orion 91–07 Triode pH/ATC probe were used to monitor the pH before and after electrochemical measurements.

An analytical rotator (Pine Instruments, model ASR) was used to control the rotation rate of the working electrode. All electrochemical experiments were performed with a Solartron model 1287 potentiostat and Corrware software (Scribner Associates) was used to control the potentiostat and record current data.

Cyclic voltammetric (CV) experiments were performed starting from –0.4 V vs. SCE (unless indicated otherwise) and scanning to +0.4V vs. SCE at a scan rate of 15 mV s^{-1}. The use of this scan rate minimized the consumption of H_2O_2. Polarization curves were recorded at a sequence of individual potentials in the range 0.1 to 0.4 V with 10 min being allowed at each potential to ensure steady-state was achieved. In corrosion experiments, E_{CORR} was recorded for 30 min at various $[CO_3]_{tot}$ and $[H_2O_2]$. The electrode was then quickly transferred to a H_2O_2-free solution to avoid interference from H_2O_2 reduction while recording a cathodic stripping voltammogram (CSV). In dissolution experiments, the working electrode was potentiostated at 0.3 V for 4 hours in a small electrochemical cell with a volume of 50 mL. Subsequently, the solution concentration of U was analyzed by inductively coupled plasma atomic emission spectroscopy (ICP-AES).

Scanning electron microscopy (SEM) and X-ray photoelectron spectroscopy (XPS) were used to analyze electrode surfaces before and after anodic oxidation. A Hitachi S-4500 (Hitachi, Japan) field emission SEM with an energy dispersive X-ray analysis (EDX) system was used at an electron acceleration voltage of 15 kV. The XPS analyzes were performed on a Kratos Axis NOVA spectrometer using a monochromatic Al K_α (1486.6 eV) source. The instrument work function was calibrated to give a binding energy of 83.96 eV for the Au $4f_{7/2}$ line for metallic gold and the spectrometer dispersion was adjusted to give a binding energy of 932.62 eV for the Cu $2p_{3/2}$ line of metallic copper. Survey scan analyzes were carried out for the energy range 0–1100 eV with an analysis area of 300 × 700 μm^2 and a pass energy of 160 eV. High resolution analyzes were carried out for the U 4f, O 1s, C 1s, and the U 5f valence band regions with an analysis area of 300 × 700 μm^2 and a pass energy of 20 eV. Spectra have been charge corrected to the main line of the C 1s spectrum (adventitious carbon) set to 285.0 eV. Spectra were analyzed using CasaXPS software (version 2.3.14) and involved a 50% Gaussian and 50% Lorentzian fitting routine with a Shirley background correction.[43] In this study, we have resolved both the two spin-orbit split peaks (U $4f_{7/2}$ and U $4f_{5/2}$) and the associated satellite structures into contributions from U^{IV}, U^{V}, and U^{VI} following the procedure described elsewhere.[18,24,44–47]

Results and Discussion

Voltammetry.— Goldik et al.[16] studied the voltammetric behavior of H_2O_2-free solutions with and without HCO_3^-/CO_3^{2-}, Fig. 1. The shallow anodic current in the potential range I was attributed to the anodic oxidation of the UO_2 matrix surface to $U^{IV}_{1-2x}U^{V}_{2x}O_{2+x}$ and the current increase at more positive potentials (II in Fig. 1) to the oxidation of this layer to a $U^{VI}O_3$ layer accompanied by dissolution as $U^{VI}O_2^{2+}$. On the reverse scan this combined layer is reduced in the potential region C_1. When HCO_3^-/CO_3^{2-} is present oxidative dissolution in region II is clearly accelerated (as $U^{VI}O_2(CO_3)_y^{(2-2y)+}$) and the smaller (almost negligible) reduction peak in the potential

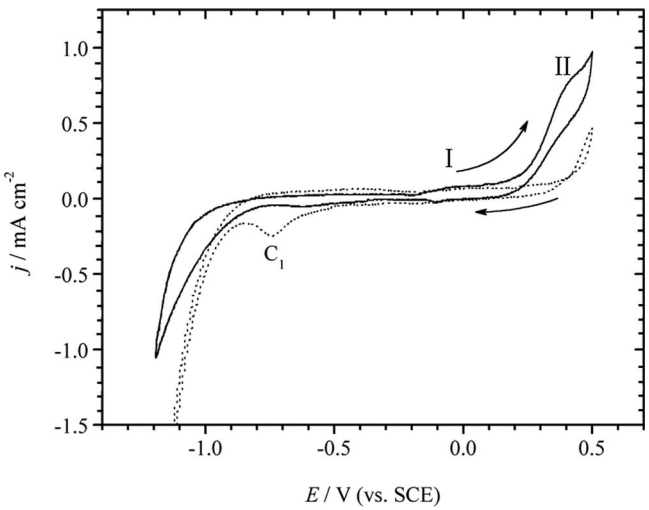

Figure 1. CVs recorded on 1.5 at% SIMFUEL in 0.1 mol L^{-1} NaCl (dashed line), and 0.1 mol L^{-1} NaCl + 0.1 mol L^{-1} Na_2CO_3/$NaHCO_3$ (solid line), both solutions at pH 9.7. Rotation rate = 16.7 Hz; scan rate = 10 mV s^{-1}. Permission to reproduce the published figure[16] is obtained.

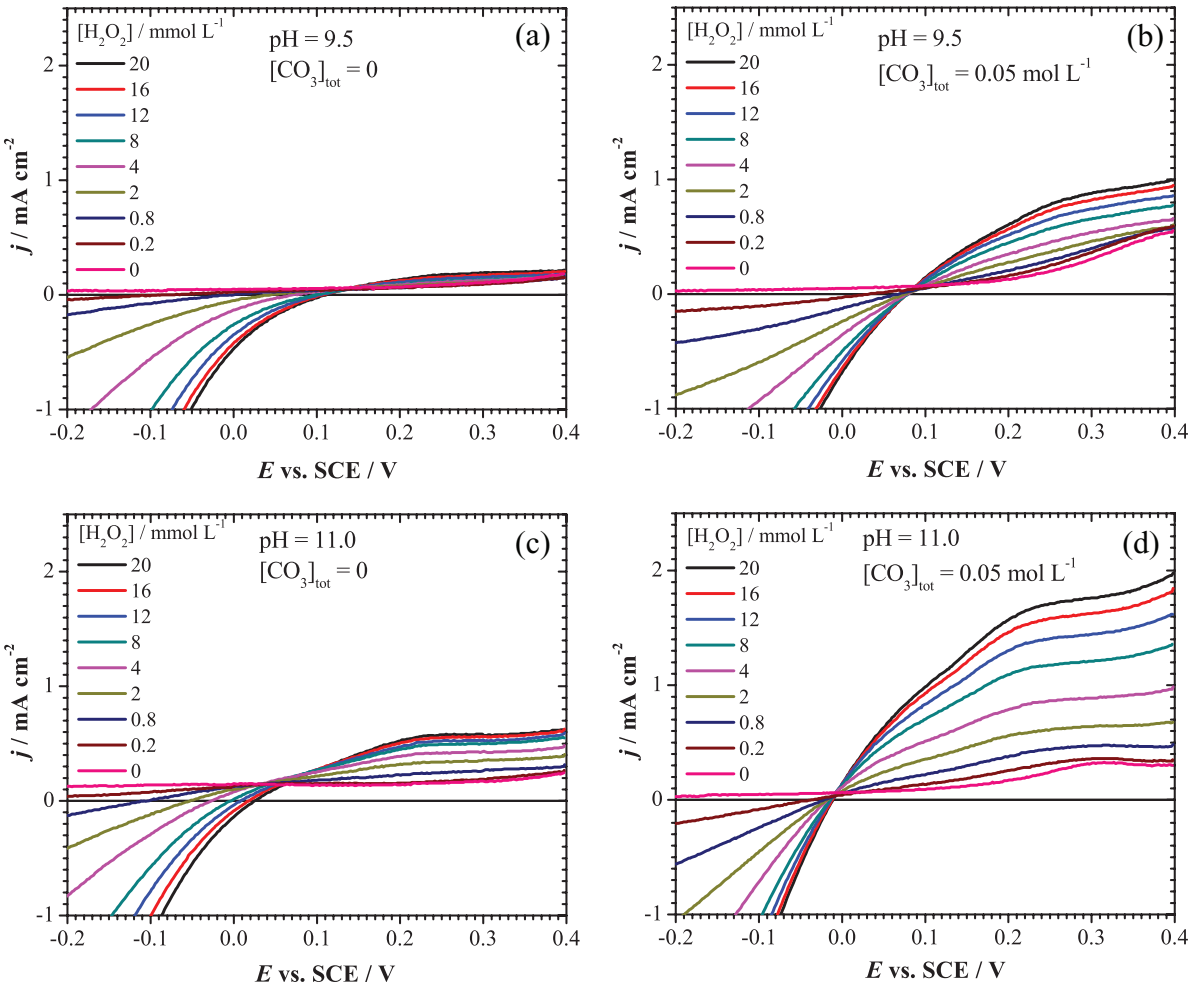

Figure 2. Current densities recorded on 1.5 at% SIMFUEL on the forward scan of CVs in 0.1 mol L^{-1} NaCl containing different $[H_2O_2]$ at pH 9.5 and 11.0; rotation rate = 25 Hz; scan rate = 15 mV s^{-1}; (a) and (c): $[CO_3]_{tot} = 0$; (b) and (d): $[CO_3]_{tot} = 0.05$ mol L^{-1}.

range –0.7 V to –0.9 V confirms that the formation of the U^{VI} layer is reduced.

A series of voltammetric measurements were performed in a HCO_3^-/CO_3^{2-}-free solution and a solution containing 0.05 mol L^{-1} HCO_3^-/CO_3^{2-} at various $[H_2O_2]$. Fig. 2 shows sections of the forward scans recorded at two pH values (9.5 and 11.0). At pH = 9.5, the cathodic reduction current readily increased with $[H_2O_2]$, while the increase in anodic current was marginal compared to the background current recorded in the absence of H_2O_2. In the presence of HCO_3^-/CO_3^{2-}, the cathodic current increased slightly probably due to the inhibition of the growth of the $U^{IV}_{1-2x}U^{V}_{2x}O_{2+x}$ layer. This effect has been studied in detail previously.[16] At pH = 9.5 in the presence of HCO_3^-/CO_3^{2-} the anodic currents increased markedly and displayed a dependence on $[H_2O_2]$. At the more alkaline pH of 11.0, the current for H_2O_2 oxidation is increased in both the absence and presence HCO_3^-/CO_3^{2-}, but particularly so in the latter case.

Fig. 3 shows the anodic currents at E = 0.4 V, after correction for the background current ($[H_2O_2]$ = 0 mol L^{-1}), taken from Fig. 2 as a function of $[H_2O_2]$. When HCO_3^-/CO_3^{2-} is present, the anodic currents became increasingly dependent on $[H_2O_2]$ compared to the values measured in HCO_3^-/CO_3^{2-}-free solutions. At the higher pH (11.0), the anodic current was directly proportional to $[H_2O_2]$ at low $[H_2O_2]$ but suppressed at $[H_2O_2]$ > 5 mmol L^{-1}. The increase in anodic current with potential can be attributed to a combination of the anodic dissolution of UO_2 and the oxidation of H_2O_2. When HCO_3^-/CO_3^{2-} is present the insulating U^{VI} surface species are chemically dissolved (as $U^{VI}O_2(CO_3)_y^{(2-2y)+}$) which exposes the underlying conductive $U^{IV}_{1-2x}U^{V}_{2x}O_{2+x}$ surface allowing enhanced electron transfer from H_2O_2. In the absence of HCO_3^-/CO_3^{2-} the dissolution rate of U^{VI} surface species (as $U^{VI}O_2(OH)_y^{(2-y)+}$) is considerably slower and both the anodic reactions are inhibited by the presence of a

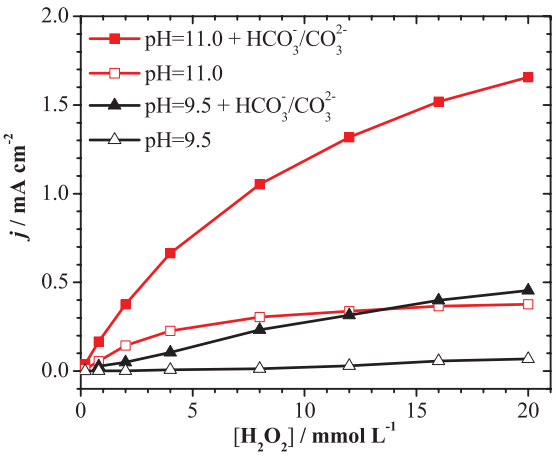

Figure 3. Anodic current densities recorded on SIMFUEL as a function of $[H_2O_2]$ in HCO_3^-/CO_3^{2-}-free/-containing solution. Data points were taken at E = 0.4 V in the CV scans (Fig. 2) and are corrected for the background current recorded in a solution without H_2O_2.

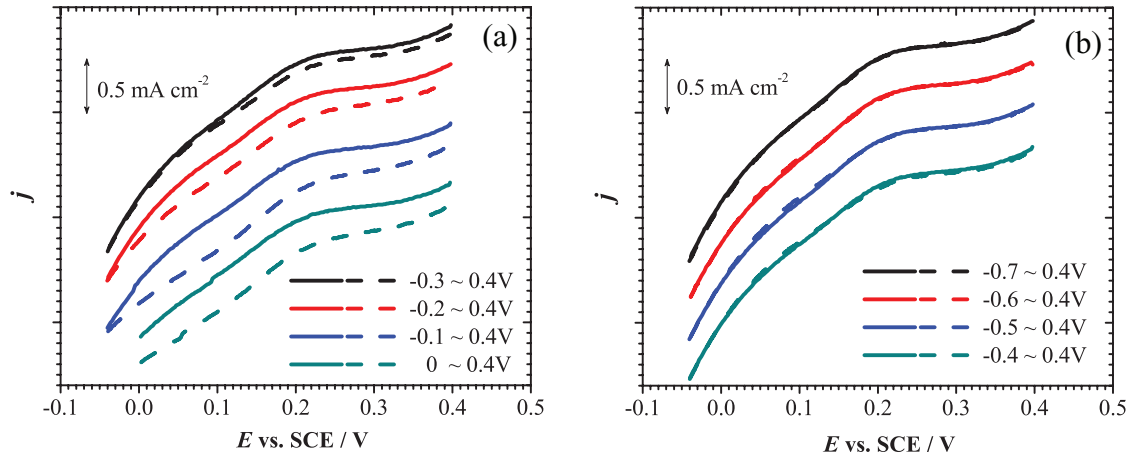

Figure 4. Anodic currents recorded on 1.5 at% SIMFUEL for various potential scan ranges. Each color indicates two consecutive scans from a specific negative potential limit. Solid lines are the 1st forward scan and dashed lines are the 2nd forward scan. [NaCl] = 0.1 mol L^{-1}; $[CO_3]_{tot}$ = 0.05 mol L^{-1}; $[H_2O_2]$ = 0.02 mol L^{-1}; pH = 11.0; rotation rate = 25 Hz; scan rate = 15 mV s^{-1}.

partially permeable U^{VI} surface oxide/hydroxide layer. This influence of pH has been discussed previously.[48] A possible explanation for the enhanced anodic current when HCO_3^-/CO_3^{2-} is present is that the oxide/hydroxide layer is either not present or considerably reduced in thickness.

To examine this possibility, a dual scan experiment was performed. The potential was scanned from various negative limits to the same positive limit (+0.4 V) and back, followed immediately by a second scan over the same potential range. The relevant sections of the forward scans are plotted in Fig. 4. A lower current on the second scan indicates that the anodic current was suppressed on the second forward scan due to the formation of an oxidized surface layer on the first scan. Providing the negative limiting potential is ≥ –0.3 V (Fig. 4a), a discrepancy exists between the anodic currents measured on the two scans confirming that the anodic reaction is inhibited by the presence of a surface film. However, this discrepancy became less significant as the cathodic limiting potential was made more negative, and was negligible once the potential was < –0.3 V (Fig. 4b). This potential dependence confirms that the anodic current up to potentials of +0.4V is inhibited by the presence of a U^{VI} layer which can be removed by cathodic reduction over the potential range –0.2 V to –0.4 V. Previously, in experiments conducted in the absence of HCO_3^-/CO_3^{2-}, the anodically formed surface layer could not be removed unless the potential at the negative limit was ≤ –0.7 V;[16] i.e., the potential range of the reduction peak C_1 in Fig. 1.

These results show the electrode surface is more readily cathodically regenerated in HCO_3^-/CO_3^{2-}, which is consistent with the absence of the reduction peak (C_1) in the CV in Fig. 1, when HCO_3^-/CO_3^{2-} was present. In the absence of HCO_3^-/CO_3^{2-} anodic oxidation processes were shown to be inhibited by a $U^{IV}_{1-2x}U^{V}_{2x}O_{2+x}/U^{VI}$ oxide/hydroxide layer. Other studies[17] have shown the $U^{IV}_{1-2x}U^{V}_{2x}O_{2+x}$ layer formed anodically is considerably thinner when HCO_3^-/CO_3^{2-} is present and these results confirm that anodic oxidation processes are limited by the presence of a U^{VI} carbonate surface layer which chemically dissolves much more rapidly than the U^{VI} oxide/hydroxide present in the absence of HCO_3^-/CO_3^{2-}, and is much more readily cathodically reduced.

Dissolution experiments.— To separate the contributions to the anodic current from the dissolution of UO_2 and the oxidation of H_2O_2, the U^{VI} content of the solution was analyzed after anodic oxidation at 0.3 V for 4 h in solutions with and without HCO_3^-/CO_3^{2-}. At this positive potential the likelihood of H_2O_2 decomposition by the coupling of its reduction and oxidation is assumed to be negligible since the reduction would be inhibited at 0.3 V based on the CVs in Fig. 2. Similarly the corrosion of UO_2 by H_2O_2 is also assumed to be negligible. The analyzed amount of UO_2^{2+} was converted to the charge required for oxidative dissolution of UO_2. Over this period of anodic oxidation the charge consumed in producing the U^{VI} carbonate layer would be negligible. The total anodic charge was obtained by integration of the measured anodic current over the time interval recorded, and the difference between the two charges can be attributed to H_2O_2 oxidation. Table I compares the values obtained in a solution free of HCO_3^-/CO_3^{2-} and in a solution containing HCO_3^-/CO_3^{2-} with two different $[H_2O_2]$. In HCO_3^-/CO_3^{2-} -free solution, a large fraction (71.5%) of the current went to H_2O_2 oxidation, and a similar fraction went to H_2O_2 oxidation in HCO_3^-/CO_3^{2-}-containing solution with the same $[H_2O_2]$ (76.8%). This similarity suggests, but does not confirm, that HCO_3^-/CO_3^{2-} promoted both H_2O_2 oxidation and UO_2 dissolution. In a solution with a lower $[H_2O_2]$ (10^{-3} mol L^{-1}), only 27.3% of anodic charge went to H_2O_2 oxidation.

Inspection of the CVs in Fig. 2c shows that (pH = 11, E = 0.3 V, $[CO_3]_{tot}$ = 0 mol L^{-1} and $[H_2O_2]$ = 0.02 mol L^{-1}) the ratio of the anodic currents in H_2O_2-free and H_2O_2-containing solutions is 0.3; i.e., 30% of the current at this potential should go to anodic oxidation/dissolution of UO_2. Considering that 71.5% of the anodic current was consumed in H_2O_2 oxidation (Table I) (i.e., 28.5% was consumed by UO_2 dissolution), the increase of current from H_2O_2-free

Table I. Distribution of charge between UO_2 oxidative dissolution and H_2O_2 oxidation.[a]

	$[CO_3]_{tot}$ = 0 mol L^{-1}, $[H_2O_2]$ = 0.02 mol L^{-1}	$[CO_3]_{tot}$ = 0.05 mol L^{-1}, $[H_2O_2]$ = 0.02 mol L^{-1}	$[CO_3]_{tot}$ = 0.05 mol L^{-1}, $[H_2O_2]$ = 0.001 mol L^{-1}
Total anodic charge (C)	0.0978	0.812	0.170
Charge due to UO_2 dissolution (C)	0.0279	0.188	0.124
Charge due to H_2O_2 oxidation (C)	0.0699	0.624	0.0464
Fraction of H_2O_2 oxidation	71.5%	76.8%	27.3%

[a]SIMFUEL electrode potentiostatically oxidized at 0.3 V for 4 h in a solution containing [NaCl] = 0.1 mol L^{-1}, pH = 11.0. No rotation was applied.

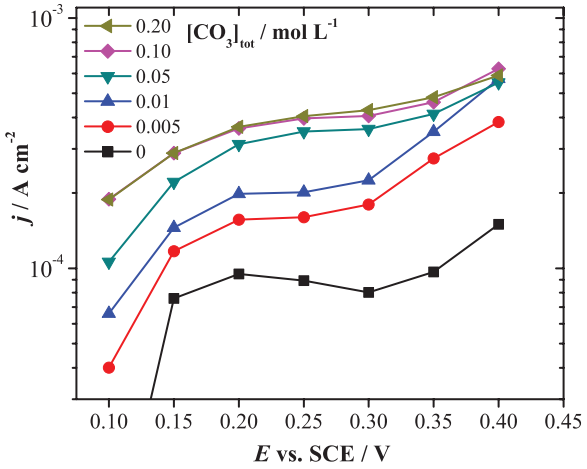

Figure 5. Tafel plots recorded on 1.5 at% SIMFUEL in solutions containing different $[CO_3]_{tot}$. [NaCl] = 0.1 mol L^{-1}; [H_2O_2] = 0.02 mol L^{-1}; pH = 9.7; rotation rate = 16.7 Hz.

to H_2O_2-containing solutions was mainly due in H_2O_2 oxidation; i.e., the addition of H_2O_2 did not significantly accelerate UO_2 dissolution. A similar comparison of currents for the HCO_3^-/CO_3^{2-} solution (Table I and Fig. 2d) showed this current ratio to be ~20%. Based on the analytical results this percentage should be 23.2%. While these results suggest a slight catalysis of UO_2 dissolution by the combination of H_2O_2 and HCO_3^-/CO_3^{2-} a more extensive analysis is required to justify this claim.

Steady-state currents at various $[CO_3]_{tot}$.— Steady-state anodic currents recorded potentiostatically at [H_2O_2] = 0.02 mol L^{-1} are plotted in the Tafel form in Fig. 5. As expected, the anodic current increased with $[CO_3]_{tot}$ over the range from 0 to 0.1 mol L^{-1} although the increase became marginal for $[CO_3]_{tot}$ > 0.05 mol L^{-1}. Also, the current was only weakly dependent on potential over the range 0.15 V to 0.30 V consistent with control of the current by the chemical dissolution of a U^{VI} surface layer ($U^{VI}O_3.yH_2O$ in the absence and $U^{VI}O_2CO_3$ in the presence of HCO_3^-/CO_3^{2-}). The increase in current for E > 0.3 V appears to be due to the oxidation of H_2O_2 on ϵ-particles and is currently under investigation.

Fig. 6 shows the anodic currents plotted against $[CO_3]_{tot}$. At the lowest potential, 0.10 V, the reaction order is 0.42, but decreases to

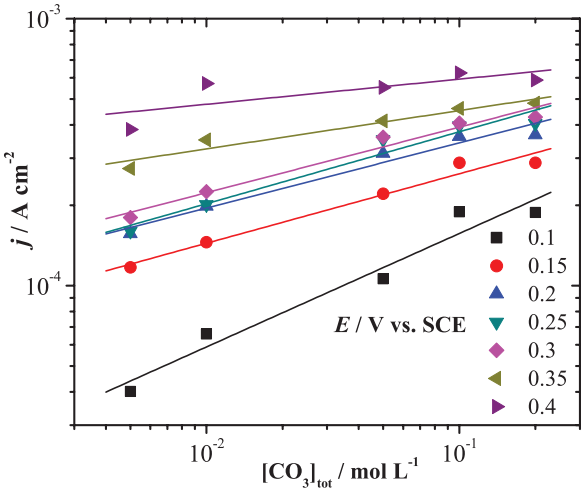

Figure 6. Plots of the anodic current densities as a function of $[CO_3]_{tot}$ at various applied potentials. (■) +0.10 V, slope = 0.42; (●) +0.15 V, slope = 0.26; (▲) +0.20 V, slope = 0.24; (▼) +0.25 V, slope = 0.27; (♦) +0.30 V, slope = 0.25; (◄) +0.35 V, slope = 0.14; (►) +0.40 V, slope = 0.09.

~0.25 over the potential range 0.15 to 0.30 V, and to 0.09 at 0.40 V. The relatively high reaction order (~0.42) with respect to $[CO_3]_{tot}$ at low potentials suggests a very significant fraction of the total anodic current can be attributed to the anodic dissolution of UO_2 which in HCO_3^-/CO_3^{2-} solution has been shown to proceed via the reaction sequence,[17]

$$UO_2 + HCO_3^- \longrightarrow (UO_2HCO_3)_{ads} + e^- \quad [1]$$

$$(UO_2HCO_3)_{ads} + OH^- \longrightarrow (UO_2CO_3)_{ads} + e^- + H_2O \quad [2]$$

$$(UO_2CO_3)_{ads} + HCO_3^- \longrightarrow [UO_2(CO_3)_2]^{2-} + H^+ \quad [3]$$

However, the decrease in reaction order at higher potentials suggests a change in dominant reaction from HCO_3^-/CO_3^{2-}-induced UO_2 dissolution to H_2O_2 oxidation. Attempts to confirm this are underway. That H_2O_2 oxidation is the dominant reaction at high potentials is confirmed by the analyzes in Table I. The influence of potential on the balance between UO_2 dissolution and H_2O_2 oxidation remains to be determined.

XPS analysis.— XPS analyzes were performed to confirm that the anodic oxidation processes were partially controlled by the presence of surface films in the potential region 0.15 V to 0.3 V. Fig. 7 shows high resolution XPS spectra for the U $4f_{5/2}$ and U $4f_{7/2}$ regions and

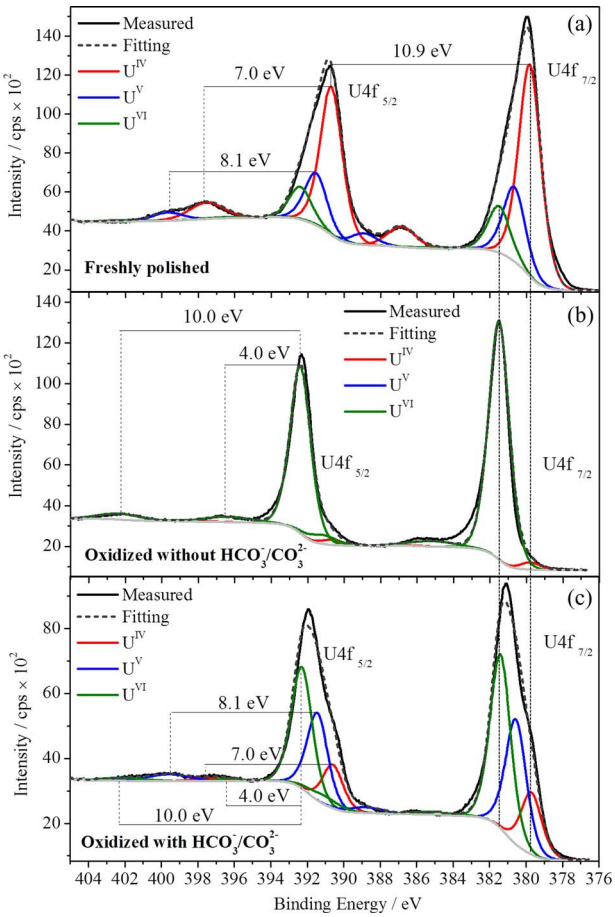

Figure 7. Resolved U $4f_{5/2}/4f_{7/2}$ regions of XPS spectra recorded on a 1.5 at% SIMFUEL surface before and after anodic oxidation at E = 0.30 V for 0.5 hour in 0.1 mol L^{-1} NaCl + 0.02 mol L^{-1} H_2O_2 at pH 11.0 with or without HCO_3^-/CO_3^{2-}. The horizontal lines indicate the separation between specific satellite peaks and the U $4f_{5/2}$ peak. (a) freshly polished specimen; (b) specimen after anodic oxidation in a HCO_3^-/CO_3^{2-}-free solution; (c) specimen after anodic oxidation in a solution containing 0.05 mol L^{-1} $Na_2CO_3/NaHCO_3$.

Table II. The fractions of U^{IV}, U^{V}, and U^{VI} in the surface of a SIMFUEL electrode before and after anodic oxidation in 0.1 mol L^{-1} NaCl + 0.02 mol L^{-1} H_2O_2, pH = 11.0.

Oxidation states	Freshly polished surface	$[CO_3]_{tot}$ = 0 mol L^{-1}		$[CO_3]_{tot}$ = 0.05 mol L^{-1}	
		0.2 V	0.3 V	0.2 V	0.3 V
U^{IV}	64%	2%	3%	23%	17%
U^{V}	22%	17%	0%	40%	35%
U^{VI}	14%	81%	97%	37%	48%

their associated satellites recorded on SIMFUEL specimens before and after oxidation at +0.3 V in a H_2O_2 containing solution with and without HCO_3^-/CO_3^{2-}. The deconvoluted U $4f_{7/2}$ peak recorded on the freshly polished electrode, Fig. 7a, shows that U^{IV} and U^{V} are the dominant oxidation states (> 85%). This is supported by the location of the satellite peaks at binding energies of 7.0 eV and 8.1 eV higher than the U $4f_{5/2}$ peak. It is possible that the small amount of U^{VI} present on the surface can be attributed to slight air oxidation of the surface on transfer to the spectrometer. The surface of the electrode anodically oxidized at +0.3 V in HCO_3^-/CO_3^{2-}-free solution (Fig. 7b) was dominated by U^{VI} (97%). This conclusion is supported by the presence of the satellite peaks at binding energies of 4.0 eV and 10.0 eV above the U($4f_{5/2}$) peak.[49–51] This analysis confirms the presence of a dominantly U^{VI} oxide/hydroxide surface layer when the anodic oxidation current is suppressed in the absence of HCO_3^-/CO_3^{2-}, Fig. 2.

This surface U^{VI} layer was considerably thinner in the presence of HCO_3^-/CO_3^{2-}, Fig. 7c, a mixture of all three oxidation states being observed. Since the U^{VI} layer formed is rapidly dissolving at 0.3 V it is likely that the measured U^{VI} content of the surface is not a true measure of the U^{VI} surface coverage when the potential was applied but reflects the difficulty in extracting the electrode from the cell without a partial loss of the U^{VI} surface layer. Table II shows the fractions of individual oxidation states determined after anodic oxidation at two potentials, +0.2 V and +0.3 V. In both the presence and absence of HCO_3^-/CO_3^{2-} the U^{VI} content of the surface is greater at the more positive potential consistent with the thickening of, or more extensive coverage by, a surface U^{VI} layer expected if the anodic current is to be independent of potential as observed, Fig. 5.

To confirm these analyzes the valence band spectra were also recorded, Fig. 8. The occupancy of the 5f level (~1 eV) is in accordance with the deconvoluted 4f spectra varying in intensity as the dominant oxidation state changes from U^{IV} to U^{VI}. These analyzes confirm that the suppression of anodic oxidation in the absence of carbonate can be attributed to the presence of a U^{VI} surface layer thick enough to obscure the underlying $U^{IV}_{1-2x}U^{V}_{2x}O_{2+x}$ layer. In the presence of HCO_3^-/CO_3^{2-} the surface remains partially blocked consistent with the potential-independent currents measured in this potential region, Fig. 2d and Fig. 5.

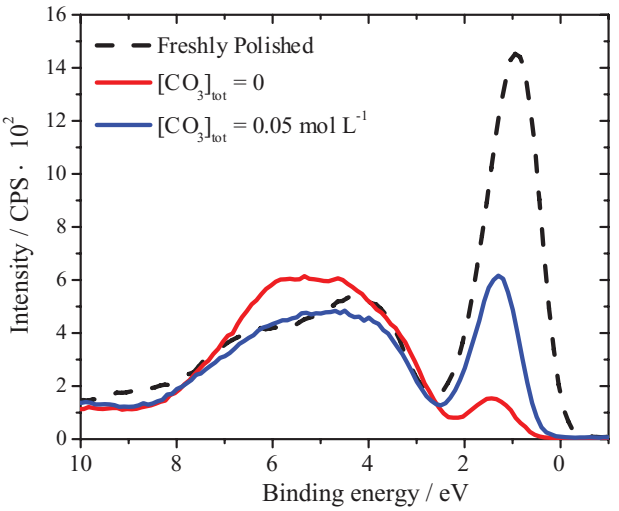

Figure 8. The valence band region of the XPS spectra recorded on a 1.5 at% SIMFUEL surface before and after anodic oxidation at E = 0.30 V for 0.5 hour in 0.1 mol L^{-1} NaCl + 0.02 mol L^{-1} H_2O_2 at pH 11.0 with or without HCO_3^-/CO_3^{2-}. Dashed line: freshly polished specimen; red line: specimen after oxidation in HCO_3^-/CO_3^{2-}-free solution; blue line: specimen after oxidation in solution containing 0.05 mol L^{-1} $Na_2CO_3/NaHCO_3$.

SEM imaging.— Fig. 9a and Fig. 9b show micrographs of the freshly polished SIMFUEL specimen. Micrographs in Fig. 9c and Fig. 9d, recorded after anodic polarization at E = 0.30 V for 1.5 hours in HCO_3^-/CO_3^{2-}-free solution, indicate little change in surface morphology had occurred, confirming the limited extent of oxidative dissolution. By contrast, after an equal period of anodic oxidation in the presence of HCO_3^-/CO_3^{2-} the electrode surface had undergone significant dissolution with the development of many etch pits and pores, Fig. 9e and Fig. 9f, consistent with the data in Table I showing the consumption of a considerable dissolution charge.

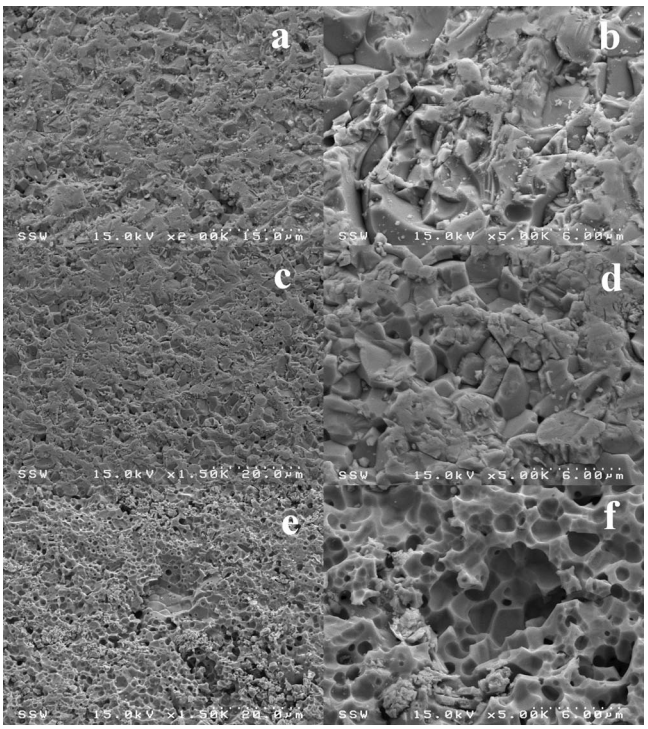

Figure 9. SEM micrographs of SIMFUEL specimens before and after anodic oxidation at E = 0.30 V for 1.5 hours in 0.1 mol L^{-1} NaCl + 0.02 mol L^{-1} H_2O_2 at pH 11.0 with or without HCO_3^-/CO_3^{2-}: (a) and (b) freshly polished specimen at 2k and 5k magnification; (c) and (d) surface after anodic oxidation in carbonate-free solution at 1.5k and 5k magnification; (e) and (f) surface after anodic oxidation in solution containing 0.05 mol L^{-1} $Na_2CO_3/NaHCO_3$ at 1.5k and 5k magnification.

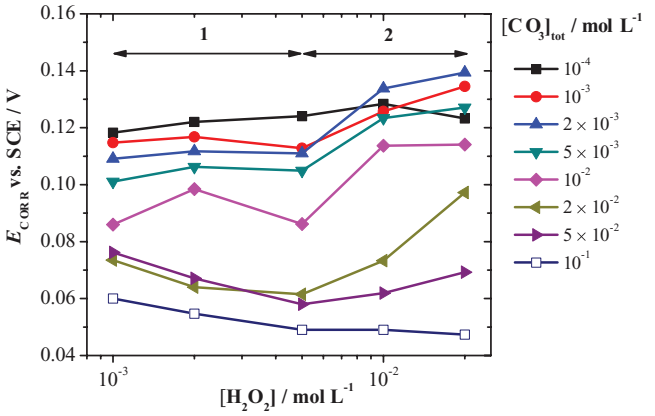

Figure 10. E_{CORR} recorded on a 1.5 at% SIMFUEL electrode as a function of $[H_2O_2]$ in 0.1 mol L^{-1} NaCl at pH = 9.5 with different $[CO_3]_{tot}$: (■) 10^{-4} mol L^{-1}; (●) 10^{-3} mol L^{-1}; (▲) 2×10^{-3} mol L^{-1}; (▼) 5×10^{-3} mol L^{-1}; (♦) 10^{-2} mol L^{-1}; (◄) 2×10^{-2} mol L^{-1}; (►) 5×10^{-2} mol L^{-1}; (□) 10^{-1} mol L^{-1}.

Open circuit experiments.— Fig. 10 shows values of E_{CORR} recorded as a function of $[H_2O_2]$ in solutions containing various $[CO_3]_{tot}$. For $[CO_3]_{tot} < 5 \times 10^{-3}$ mol L^{-1}, E_{CORR} values decrease with increasing $[CO_3]_{tot}$ and show a similar dependence on $[H_2O_2]$ to that observed in the absence of HCO_3^-/CO_3^{2-};[15] i.e., E_{CORR} is independent of $[H_2O_2]$ for $[H_2O_2] \leq 5 \times 10^{-3}$ mol L^{-1} (region 1 in Fig. 10) but increases at higher $[H_2O_2]$ (region 2 in Fig. 10). As the $[CO_3]_{tot}$ is increased further, E_{CORR} values decrease substantially indicating a possible depolarization of the UO_2 corrosion rate. The E_{CORR} values maintain the differences between the two $[H_2O_2]$ ranges up to 2×10^{-2} mol L^{-1} $[CO_3]_{tot}$ but at higher $[CO_3]_{tot}$ employed (e.g. 10^{-1} mol L^{-1}) E_{CORR} varies by ~12 mV over the whole $[H_2O_2]$ range.

Fig. 11 and Fig. 12 show the fractions of individual oxidation states as a function of $[H_2O_2]$ recorded in a solution free of HCO_3^-/CO_3^{2-}, Fig. 11, and in a solution containing the maximum $[CO_3]_{tot}$ used in the separate series of E_{CORR} measurements (Fig. 10), Fig. 12. In the absence of HCO_3^-/CO_3^{2-}, Fig. 11, the fraction of U^{VI} on the electrode surface remained effectively independent of $[H_2O_2]$ over the potential region 1 (Fig. 10) when E_{CORR} does not change before increasing in potential region 2 (Fig. 10) as E_{CORR} increases. This

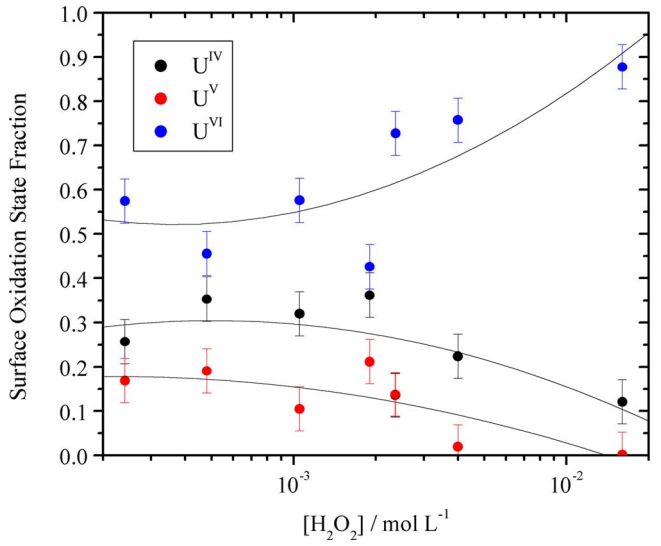

Figure 11. The fraction of individual oxidation states present in the surface of a 1.5 at% SIMFUEL electrode as a function of the H_2O_2 concentration in 0.1 mol L^{-1} NaCl at pH 9.7; (●) U^{IV}; (●) U^{V}; (●) U^{VI}.

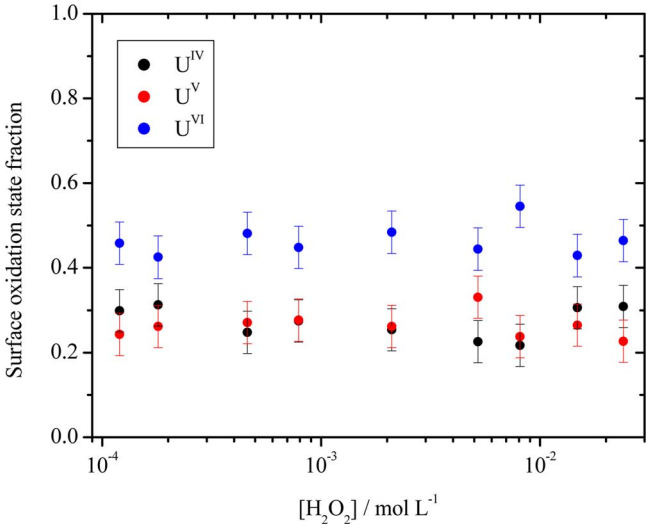

Figure 12. The fraction of individual oxidation states present in the surface of a 1.5 at% SIMFUEL electrode as a function of the $[H_2O_2]$ in 0.1 mol L^{-1} NaCl + 0.1 mol L^{-1} Na_2CO_3/$NaHCO_3$ at pH 9.7; (●) U^{IV}; (●) U^{V}; (●) U^{VI}.

behavior confirms that observed previously,[15] and would be consistent with dissolution controlled by slow U^{VI} release in potential region 1 evolving to localized dissolution at acidified locations in the surface asperities (Fig. 9c and 9d) on a more extensively covered U^{VI} surface at higher $[H_2O_2]$.

In the presence of $[CO_3]_{tot} = 0.1$ mol L^{-1}, Fig. 12, the fractions of the individual oxidation states in the electrode surface did not change with $[H_2O_2]$ and the U^{VI} fraction was significantly lower than that observed in the absence of HCO_3^-/CO_3^{2-}, especially at the higher $[H_2O_2]$. This behavior suggests that this $[CO_3]_{tot}$ (0.1 mol L^{-1}) prevents the accumulation of the U^{VI} surface layer leading to the blockage of the electrode surface observed in the anodic polarization scans in Fig. 2.

CSV measurements.— To confirm the influence of HCO_3^-/CO_3^{2-}, CSV experiments were performed after the E_{CORR} measurements (Fig. 10). Fig. 13 shows the CSVs recorded after corrosion in 0.02 mol L^{-1} H_2O_2 in solutions with different $[CO_3]_{tot}$. At the two low concentrations a significant reduction peak, indicating the presence of a substantial U^{VI} surface layer, is observed. As expected from the CV in Fig. 1 this peak is located in the potential range −0.65 V to –0.85 V and can be attributed to the cathodic reduction

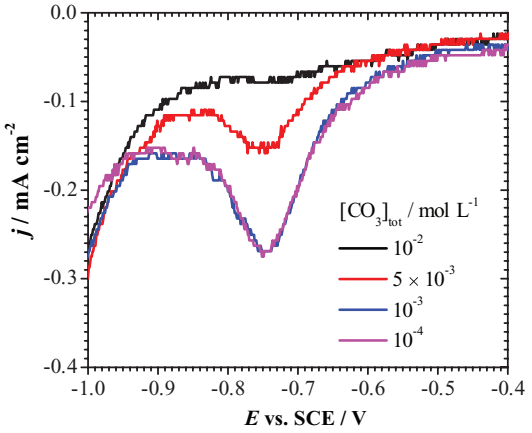

Figure 13. CSVs recorded on a SIMFUEL electrode after 30 min of E_{CORR} measurement in 0.02 mol L^{-1} H_2O_2 and various $[CO_3]_{tot}$ at pH = 9.5.

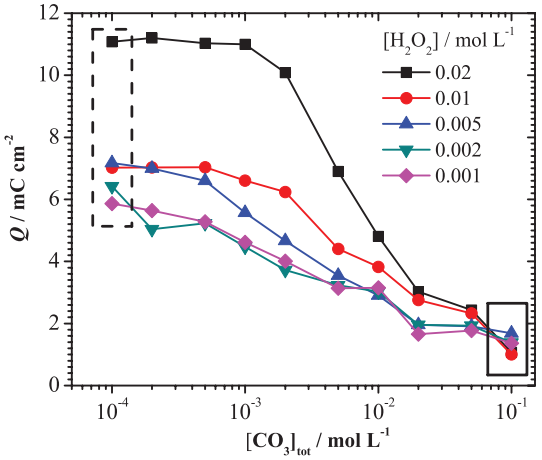

Figure 14. The surface charge (proportional to the thickness of the corrosion product layer) on a SIMFUEL surface as a function of $[CO_3]_{tot}$ in solutions containing different $[H_2O_2]$: (■) 2×10^{-2} mol L^{-1}; (●) 10^{-2} mol L^{-1}; (▲) 5×10^{-3} mol L^{-1}; (▼) 2×10^{-3} mol L^{-1}; (♦) 10^{-3} mol L^{-1}.

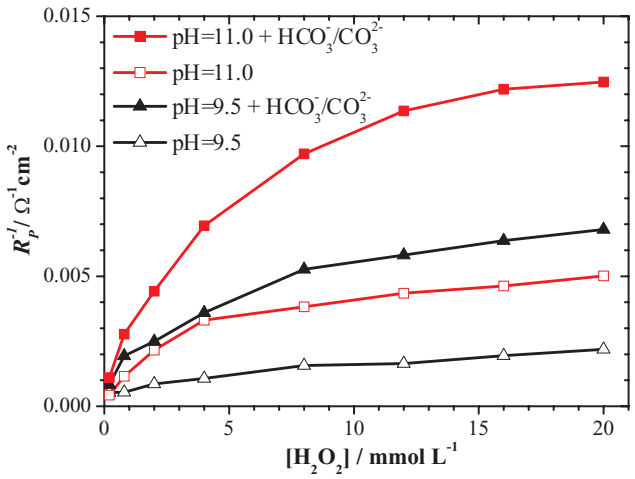

Figure 15. Reciprocal of polarization resistance, R_P^{-1}, as a function of $[H_2O_2]$ at pH 9.5 and 11.0. $[CO_3]_{tot}$ = 0 or 0.05 mol L^{-1}, rotation rate = 25 Hz.

of a $U^{IV}_{1-2x}U^{V}_{2x}O_{2+x}/U^{VI}O_3.yH_2O$ layer formed by corrosion in the H_2O_2 solution. As the $[CO_3]_{tot}$ is increased the size of this peak decreases with only a very shallow peak being observed at the highest $[CO_3]_{tot}$. A reasonable estimate of the extent of formation of this U^{VI} surface layer can be obtained by integrating the CSVs between –0.6 V and –0.9 V to obtain the charge associated with the cathodic reduction of this film. The charges obtained in this manner are plotted for the whole series of corrosion experiments in Fig. 14.

Fig. 14 shows the extent of surface oxidation (expressed as a surface charge) calculated from the integration of the stripping current from –0.9 V to –0.6 V as a function of $[CO_3]_{tot}$. In the solution with the lowest $[CO_3]_{tot}$ (10^{-4} mol L^{-1} as shown in the dashed box) the charge is almost independent of $[H_2O_2]$ up to 0.01 mol L^{-1} but increased significantly for $[H_2O_2]$ = 0.02 mol L^{-1}. This trend is consistent with the XPS results which show U^{VI} becoming the dominant surface oxidation state at high $[H_2O_2]$ (Fig. 11). By contrast the surface charge at the highest $[CO_3]_{tot}$ (0.1 mol L^{-1}) (solid box in Fig. 14) is very low and independent of $[H_2O_2]$. This low charge together with the low U^{VI} content of the surface is consistent with the presence of a rapidly dissolving, and hence difficult to capture by ex-situ XPS analysis, thin layer of U^{VI} carbonate.

Over the intermediate $[CO_3]_{tot}$ range the surface charge decreases with increasing $[CO_3]_{tot}$. This range (10^{-3} to $\sim 2 \times 10^{-2}$ mol L^{-1}) is independent of $[H_2O_2]$. These data demonstrate that whether or not the surface accumulates a U^{VI} deposit depends on the relative rates of surface oxidation (R_H determined by $[H_2O_2]$) and chemical dissolution of U^{VI} states (R_U determined by $[CO_3]_{tot}$). For $[CO_3]_{tot} \leq 10^{-3}$ mol L^{-1}, $R_H > R_U$, while the opposite is the case at high $[CO_3]_{tot}$.

Polarization resistance measurements.— Using the plots in Fig. 2, it is possible to measure a polarization resistance (R_P) for charge transfer reactions occurring at E_{CORR} by measuring the slope of the current-potential plots over the range $E_{CORR} \pm 10$ mV. Since two open circuit reactions are possible, UO_2 corrosion and H_2O_2 decomposition, any measured R_P value is a measure of the resistance to charge transfer of the sum of these two reactions. Values of R_P^{-1} measured as a function of $[H_2O_2]$ in solutions with and without HCO_3^-/CO_3^{2-} at pH = 9.5 and 11.0 are plotted in Fig. 15.

Presently, the open circuit balance between these two reactions is unknown and may change with $[H_2O_2]$ as observed under anodic polarization conditions (Table I). These results showed that the relative importance of the H_2O_2 decomposition reaction decreased as $[H_2O_2]$ decreased. At the relatively high $[H_2O_2]$ of 0.02 mol L^{-1} these analyzes show that ~75% of the current goes to H_2O_2 decomposition under electrochemical conditions.

If a similar balance between dissolution and decomposition is assumed to prevail at E_{CORR} then the reciprocal of the polarization resistance, R_P^{-1}, can be taken as an approximate measure of the H_2O_2 decomposition rate, at least for higher $[H_2O_2]$ when Fig. 15 shows R_P^{-1} values to be effectively independent of $[H_2O_2]$. Irrespective of these difficulties it is clear that an increase in both pH and $[CO_3]_{tot}$ increases the rate of H_2O_2 decomposition. Previously in the absence of HCO_3^-/CO_3^{2-} this was attributed to a combination of the increased rate of dissolution of the inhibiting U^{VI} surface layer (as $U^{VI}O_2(OH)_y^{(2-y)+}$) and an increase in concentration of the electroactive form of peroxide, HO_2^- (by H_2O_2 dissociation).[48] However, the data in Fig. 15 show that the rate of interfacial reaction (R_P^{-1}) can be increased by adding HCO_3^-/CO_3^{2-} without changing the pH. This would suggest that the rate of chemical dissolution of U^{VI} species (as $U^{VI}O_2(CO_3)_x^{(2-2x)+}$) is the key feature controlling the surface reactivity. However, since a similar but smaller increase in R_P^{-1} is observed by changing the pH at the same $[CO_3]_{tot}$ the possibility remains that HO_2^- is more electroactive than H_2O_2.

Conclusions

The anodic behavior of SIMFUEL in solutions containing H_2O_2 and HCO_3^-/CO_3^{2-} has been studied electrochemically and using surface analytical techniques. Two anodic reactions are possible: the dissolution of UO_2 and the oxidation of H_2O_2.

In the absence of HCO_3^-/CO_3^{2-}, the dissolution rate of U^{VI} (as $U^{VI}O_2(OH)_y^{(2-y)+}$) is slow and both anodic reactions are inhibited by the presence of a partially permeable U^{VI} surface oxide/hydroxide layer. When HCO_3^-/CO_3^{2-} is present the more rapid chemical dissolution of U^{VI} (as $U^{VI}O_2(CO_3)_x^{(2-2x)+}$) exposes the underlying conductive $U^{IV}_{1-2x}U^{V}_{2x}O_{2+x}$ surface which facilitates the anodic oxidation of H_2O_2.

The dependencies of the anodic current on $[CO_3]_{tot}$ and $[H_2O_2]$ indicate that the rate of anodic dissolution increases at potentials positive to the open circuit (corrosion) potential, but at higher potentials when the dissolution rate is limited by the chemical release of U^{VI}, the anodic oxidation of H_2O_2 is the dominant reaction. It is possible that both anodic reactions are dependent on $[H_2O_2]$ due to the formation of a uranyl peroxocarbonate complex ($U^{VI}O_2(O_2)_x(CO_3)_y^{2-2x-2y}$) although this remains to be conclusively demonstrated.

Under open circuit (corrosion) conditions both UO_2 corrosion and H_2O_2 decomposition are controlled by the rate of chemical release of U^{VI} surface species. Since the rate of release is accelerated in

the presence of HCO_3^-/CO_3^{2-} the rates of both reactions increase with $[CO_3]_{tot}$. This is clearly indicated in polarization resistance measurements. However, such measurements cannot distinguish between these two reactions and studies to quantitatively separate them are underway.

Acknowledgments

This research was funded under the Industrial Research Chair agreement between the Natural Science and Engineering Research Council (NSERC, Ottawa) and the Nuclear Waste Management Organization (NWMO, Toronto). Surface Science Western is acknowledged for the use of their XPS and SEM equipment. The authors also thank Dr. Mark Biesinger for the help with XPS, Heather Bloomfield for the help with SEM, and Dr. Charles Wu for conducting the ICP test in Biotron. Regrettably, author Jon S. Goldik passed away before this article was published.

References

1. J. McMurry, D. A. Dixon, J. D. Garroni, B. M. Ikeda, S. Stroes-Gascoyne, P. Baumgartner, and T. W. Melnyk, *Ontario Power Generation*, Report 06819-REP-01200-10092-R00, Toronto, ON (2003).
2. F. King and M. Kolar, *Ontario Power Generation*, Report 06819-REP-01200-10041-R00, Toronto, ON (2000).
3. F. King, C. Lilja, K. Pedersen, P. Pitkänen, and M. Vähänen, *Swedish Nuclear Fuel and Waste Management Co. (SKB)*, Report TR-10-67, Stockholm, Sweden (2010).
4. I. Grenthe, J. Fuger, R. J. Konings, R. J. Lemire, A. B. Muller, C. Nguyen-Trung, and H. Wanner, *Chemical Thermodynamics of Uranium*, North Holland, Armsterdam (1992).
5. D. W. Shoesmith, *J. Nucl. Mater.*, **282**, 1 (2000).
6. E. Ekeroth, O. Roth, and M. Jonsson, *J. Nucl. Mater.*, **355**(1–3), 38 (2006).
7. C. M. Lousada, M. Trummer, and M. Jonsson, *J. Nucl. Mater.*, **434**, 434 (2013).
8. J. McMurry, *Ontario Power Generation*, Report 06819-REP-01200-10135-R01, Toronto, ON (2004).
9. I. Grenthe, D. Ferri, F. Salvatore, and G. Riccio, *J. Chem. Soc. Dalton Trans.*, **11**, 2439 (1984).
10. D. W. Shoesmith, S. Sunder, and W. H. Hocking, in *Electrochemistry of Novel Materials*, J. Lipkowski and P. N. Ross, eds., Vol. 297, VCH publishers, New York (1994).
11. M. Hossain, E. Ekeroth, and M. Jonsson, *J. Nucl. Mater.*, **358**(2-3), 202 (2006).
12. J. de Pablo, I. Casas, J. Gimenez, V. Marti, and M. E. Torrero, *J. Nucl. Mater.*, **232**, 138 (1996).
13. J. de Pablo, I. Casas, J. Gimenez, M. Molera, M. Rovira, L. Duro, and J. Bruno, *Geochim. Cosmochim. Acta*, **63**, 3097 (1999).
14. S. Röllin, K. Spahiu, and U. B. Eklund, *J. Nucl. Mater.*, **297**(3), 231 (2001).
15. S. Sunder, N. H. Miller, and D. W. Shoesmith, *Corros. Sci.*, **46**(5), 1095 (2004).
16. J. S. Goldik, J. J. Noël, and D. W. Shoesmith, *Electrochim. Acta*, **51**(16), 3278 (2006).
17. P. G. Keech, J. S. Goldik, Z. Qin, and D. W. Shoesmith, *Electrochim. Acta*, **56**, 7923 (2011).
18. B. G. Santos, H. W. Nesbitt, J. J. Noël, and D. W. Shoesmith, *Electrochim. Acta*, **49**, 1863 (2004).
19. J. S. Goldik, H. W. Nesbitt, J. J. Noël, and D. W. Shoesmith, *Electrochim. Acta*, **49**(11), 1699 (2004).
20. J. Gimenez, E. Baraj, M. E. Torrero, I. Casas, and J. de Pablo, *J. Nucl. Mater.*, **238**, 64 (1996).
21. J. S. Goldik, J. J. Noël, and D. W. Shoesmith, *J. of Electroanal. Chem.*, **582**(1-2), 241 (2005).
22. M. Trummer, S. Nilsson, and M. Jonsson, *J. Nucl. Mater.*, **378**(1), 55 (2008).
23. B. G. Santos, J. J. Noël, and D. W. Shoesmith, *J. of Electroanal. Chem.*, **586**, 1 (2006).
24. M. Razdan, Vol. PhD Thesis. Western University, London, ON, 2013.
25. H. Christensen and E. Bjergbakke, (eds.), *Radiation induced dissolution of UO_2*, Material Research Society, Pittsburgh (1987).
26. J. C. Wren, D. W. Shoesmith, and S. Sunder, *J. Electrochem. Soc.*, **152**(11), B470 (2005).
27. S. M. Peper, L. F. Brodnax, S. E. Field, R. A. Zehnder, S. N. Valdez, and W. H. Runde, *Ind. Eng. Chem. Res.*, **43**, 8188 (2004).
28. G. S. Goff, L. F. Brodnax, M. R. Cisneros, S. M. Peper, S. E. Field, B. L. Scott, and W. H. Runde, *Inorg. Chem.*, **47**, 1984 (2008).
29. H. Christensen, R. Forsyth, R. Lundqvist, and L. O. Werme, *Studsvik Energiteknik AB*, Report NS-90/85, Nyköping, Sweden (1990).
30. P. Diaz-Arocas, J. Quinones, C. Maffiotte, J. Serrano, J. Garcia, and J. R. Almazan, *Mater. Res. Soc. Symp. Proc.*, **353**, 641 (1995).
31. J. de Pablo, I. Casas, F. Clarens, F. El Aamrani, and M. Rovira, *Mat. Res. Soc. Symp. Proc.*, **663**, 409 (2001).
32. M. Jonsson, E. Ekeroth, and O. Roth, *Mater. Res. Soc. Symp. Proc.*, **807**, 77 (2004).
33. R. Pehrman, M. Trummer, C. M. Lousada, and M. Jonsson, *J. Nucl. Mater.*, **430**, 6 (2012).
34. S. Nilsson and M. Jonsson, *J. Nucl. Mater.*, **410**, 89 (2011).
35. H. M. Cota, T. Katan, M. Chin, and F. J. Schoenweis, *Nature*, **203**, 1281 (1964).
36. J. A. Navarro, M. A. de la Rosa, M. Roncel, and F. de la Rosa, *J. Chem. Soc. Faraday Trans. 1.*, **80**, 249 (1984).
37. L. J. Csanyi and Z. M. Galbacs, *J. Chem. Soc. Faraday Trans. 1.*, **81**, 113 (1985).
38. H. H. B. Lee, A.-H. Park, and C. Oloman, *TAPPI Journal*, **83**, August Issue (2000).
39. D. E. Richardson, H. Yao, K. M. Frank, and D. A. Bennett, *J. Am. Chem. Soc.*, **122**, 1729 (2000).
40. H. U. Suess and M. Janik, Technical Articles, Technical Association of the Pulp and Paper Industry of Southern Africa/TAPPSA, http://www.tappsa.co.za/technical_articles.html, accessed (2009).
41. T. Wu and J. D. Englehardt, *Environ. Sci. Technol.*, **46**, 2291 (2012).
42. D. W. Shoesmith, W. H. Hocking, S. Sunder, J. S. Betteridge, and N. H. Miller, *J. Alloys Compd.*, **213/214**, 551 (1994).
43. D. A. Shirley, *Phys. Rev. B*, **5**(12), 4709 (1972).
44. M. Schindler, F. C. Hawthorne, M. S. Freund, and P. C. Burns, *Geochim. Cosmochim. Acta*, **73**, 2471 (2009).
45. E. S. Ilton, A. Haiduc, C. L. Cahill, and A. R. Felmy, *Inorg. Chem.*, **44**, 2986 (2005).
46. E. S. Ilton, J.-F. Boily, and P. S. Bagus, *Surface Science*, **601**, 908 (2007).
47. M. Razdan, D. S. Hall, P. G. Keech, and D. W. Shoesmith, *Electrochim. Acta*, **83**, 410 (2012).
48. L. Wu and D. W. Shoesmith, *Electrochim. Acta*, Submitted (2014).
49. Y. A. Teterin, V. M. Kulakov, A. S. Baev, N. B. Nevzorov, I. V. Melnikov, V. A. Streltsov, L. G. Mashirov, D. N. Suglobov, and A. G. Zelenkov, *Physics and Chemistry of Minerals*, **7**, 151 (1981).
50. S. Bera, S. K. Sali, S. Sampath, S. V. Narasimhan, and V. Venugopal, *J. Nucl. Mater.*, **255**, 26 (1998).
51. S. Van den Berghe, J.-P. Laval, B. Gaudreau, H. Terryn, and M. Verwerft, *J. Nucl. Mater.*, **277**, 28 (2000).